

High-Energy Limit of Massless Dirac Fermions in Multilayer Graphene using Magneto-Optical Transmission Spectroscopy

P. Plochocka,* C. Faugeras, M. Orlita, M.L. Sadowski, G. Martinez, and M. Potemski
Grenoble High Magnetic Field Laboratory, CNRS, 38042 Grenoble, France

M.O. Goerbig and J.-N. Fuchs
Laboratoire de Physique des Solides, CNRS UMR 8502, Univ. Paris-Sud, F-91405 Orsay cedex, France

C. Berger and W.A. de Heer
Georgia Institute of Technology, Atlanta, Georgia, USA

(Dated: October 23, 2018)

We have investigated the absorption spectrum of multi-layer graphene in high magnetic fields. The low-energy part of the spectrum of electrons in graphene is well described by the relativistic Dirac equation with a linear dispersion relation. However, at higher energies (> 500 meV) a deviation from the ideal behavior of Dirac particles is observed. At an energy of 1.25 eV, the deviation from linearity is $\simeq 40$ meV. This result is in good agreement with the theoretical model, which includes trigonal warping of the Fermi surface and higher order band corrections. Polarization-resolved measurements show no observable electron-hole asymmetry.

PACS numbers: 78.67.-n, 73.21.-b

Graphene, a single sheet of graphite, is a two-dimensional system which exhibits unique electronic properties mostly related to its peculiar band structure [1, 2, 3, 4]. The remarkable physics exhibited by graphene has its origin in the conduction and the valence bands which meet at the two inequivalent (K and K') corners of the Brillouin zone. The electrons in the vicinity of the Fermi energy do not obey Schrödinger's equation, but should instead be described using the quantum-electrodynamic Dirac equation for relativistic fermions with zero rest mass. The electrons have a linear dispersion relation whose slope defines a Fermi velocity v_F . In a relativistic analogy, these electrons behave as massless Dirac fermions moving at an effective speed of light v_F . This system is of great interest from a fundamental physics point of view and it has even been suggested that graphene can be used for bench top quantum electrodynamics experiments [1], for example to test the Klein paradox [5]. However, in graphene, considering the carriers as massless fermions remains an approximation and it is both important and interesting to verify the limits of this approximation.

Graphene has been extensively investigated using optical measurements such as Raman scattering [6, 7, 8, 9], far-infrared absorption (FIR) [10, 11], as well as magneto-photoconductivity [12]. Landau level (LL) spectroscopy is a direct and precise tool to test the linear dispersion relation in the close vicinity of the K and K' points of the Brillouin zone. In the presence of a magnetic field B , perfect linearity leads to the observed \sqrt{Bn} spacing for the LLs indexed by the integer n . In the low-energy range of the Dirac cone, the linearity of the dispersion relation is well preserved [10, 11, 12]. However, graphene is a solid-state system composed of carbon atoms arranged

in a honeycomb lattice and the linear dispersion in these specific high symmetry points is only a part of a complicated band structure. This implies that the analogy with neutrinos, massless Dirac particles, cannot hold everywhere, and we expect a deviation from a linear dispersion for high energies of the Dirac cone. Although it is well established that at low energies, electrons in graphene can be treated as massless Dirac particles, it is crucial to determine the limits of this approach.

In this Letter, we probe the limits of the massless Dirac fermion approximation in graphene by extending the previous studies [10, 13] to higher magnetic fields, and, most importantly, to higher energies. Using magneto-optical transmission spectroscopy, we present a full LL spectroscopy in magnetic fields up to 32 T, from the far infrared to the visible range of energy. Transmission measurements performed in the near visible provide an access to the high-energy range (≤ 1.25 eV) of the Dirac cone. A significant deviation from the linear dispersion of ideal Dirac fermions is observed. The experimental data are compared to a theoretical model which includes higher-order band terms and a good agreement is obtained. In addition, the asymmetry between electrons and holes has been probed using polarization-resolved transmission experiments.

We have investigated samples containing a high number of graphene layers (between 70 and 100) grown in vacuum by the thermal decomposition method, on a (4H) SiC [14, 15] substrate. Both experiment and theory confirm that the layers are electronically decoupled so that the system can be considered as a multi-layer graphene sample [9, 10, 13, 16]. In particular, these samples show Raman spectra with the characteristic signature of single layer graphene [9]. It is likely that this peculiar-

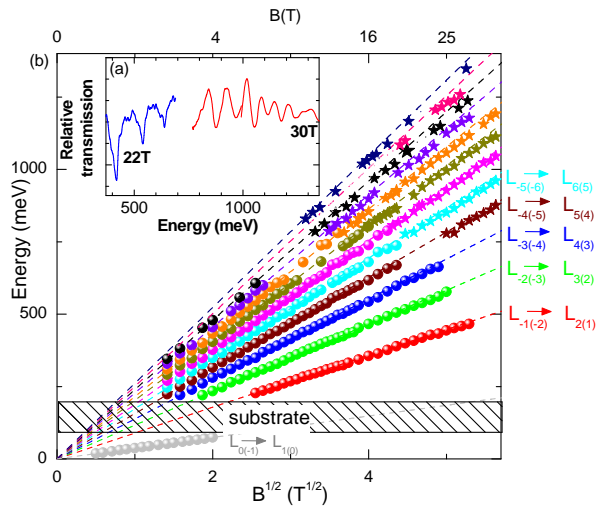


FIG. 1: (color online) (a) Representative differential transmission spectra (the $B = 0$ T spectra has been subtracted) measured at the given magnetic fields. (b) Positions of the absorption lines as a function of the square root of the magnetic field. Stars represent data obtained in near visible range, circles denotes the data measured by FTS. Dashed lines are calculated energy of the transitions between LLs assuming a linear dispersion. On the right hand side the observed transition $L_{-m(-n)} \rightarrow L_{n(m)}$ LLs are denoted.

ity of multi-layer graphene, as compared to graphite, is due to rotational disorder in the stacking, which reduces strongly the interlayer coupling by roughly two orders of magnitude [16]. To cover the full spectral range, two different experiments have been performed. The unpolarized far-infrared magneto-transmission of the sample at $T = 1.9$ K has been measured using a Fourier Transform Spectroscopy (FTS). To explore the higher energy range the magneto-transmission up to the visible light range has been measured at $T = 4.2$ K using a tungsten halogen lamp. Transmission measurements were circular polarization resolved and spectra recorded for both polarities of the magnetic field. A representative transmission spectra is shown in Fig. 1(a). All spectra show a number of absorption lines which can be assigned to transitions between $L_{-m(-n)}$ and $L_{n(m)}$ LLs, where m, n enumerates the Landau levels. In the experiment, we observed all transitions from $L_{-1} \rightarrow L_2$ ($L_{-2} \rightarrow L_1$) to $L_{-13} \rightarrow L_{12}$ ($L_{-12} \rightarrow L_{13}$).

The energetic position of the observed absorption lines is plotted as a function of the square root of the magnetic field in Fig 1(b). At low energies, the positions of the optical transitions follow the theoretical (linear) prediction for Dirac particles [dashed lines in Fig 1(b)]. For energies above ~ 500 meV a deviation from the predicted linear Dirac dispersion starts to be observed (this can be seen more clearly in Fig. 2). Recently Jiang *et al.* [11] presented FIR spectra of a single layer of exfoliated graphene

and determined a Fermi velocity $v_F = 1.1 \times 10^6$ m/s. This is somewhat larger than the value $v_F = 1.02 \times 10^6$ m/s obtained here from the slope in the low-energy region of Fig. 1(b). Moreover, in Ref. [11], a deviation from the ideal scaling between adjacent energy transitions was reported, and interpreted as a consequence of electron-electron interactions. In contrast, in our data the scaling of the transition energies is well preserved in the low energy part of the Dirac cone [see Fig1(b)], while at higher energies, we observe deviations due to the non-linearity of the dispersion relation, as discussed below.

A simple theoretical model has been developed to investigate deviations from the relativistic Dirac case within the tight-binding model with a nearest-neighbor (n.n.) hopping term $t \approx 3$ eV on a honeycomb lattice [17]. Next-nearest-neighbor (n.n.n.) hopping t' , between sites on the same sublattice, is also included, with $t'/t \sim 0.1$ [18]. The model considers a single graphene layer, which is a valid assumption in the case of almost decoupled layers. The energy dispersion for this model may be obtained from a diagonalization of the 2×2 Hamiltonian matrix, which reflects the presence of two triangular sublattices A and B ,

$$\mathcal{H}(\mathbf{q}) = \begin{pmatrix} h'(\mathbf{q}) & h^*(\mathbf{q}) \\ h(\mathbf{q}) & h'(\mathbf{q}) \end{pmatrix}, \quad (1)$$

with $h(\mathbf{q}) \equiv -t \sum_{j=1}^3 \exp(i\mathbf{q} \cdot \mathbf{a}_j)$ and $h'(\mathbf{q}) \equiv 2t' \sum_{j=1}^3 \cos(\mathbf{q} \cdot \boldsymbol{\tau}_j)$. Here, the vectors $\mathbf{a}_1 = \tilde{a}(\sqrt{3}\mathbf{e}_x + \mathbf{e}_y)/2$, $\mathbf{a}_2 = \tilde{a}(-\sqrt{3}\mathbf{e}_x + \mathbf{e}_y)/2$, and $\mathbf{a}_3 = -\tilde{a}\mathbf{e}_y$ indicate the coordinates of n.n. carbon atoms, with a distance $\tilde{a} = 0.14$ nm, and $\boldsymbol{\tau}_1 = \sqrt{3}\tilde{a}\mathbf{e}_x$, $\boldsymbol{\tau}_2 = \sqrt{3}\tilde{a}(\mathbf{e}_x + \sqrt{3}\mathbf{e}_y)/2$, and $\boldsymbol{\tau}_3 = \sqrt{3}\tilde{a}(-\mathbf{e}_x + \sqrt{3}\mathbf{e}_y)/2$ those between n.n.n.

In order to obtain the low-energy spectrum of the dispersion, one expands $h(\mathbf{q})$ and $h'(\mathbf{q})$ around the K and K' points at the edges of the first Brillouin zone (BZ), characterized by the wave vectors $\pm\mathbf{K} = \pm(4\pi/3\sqrt{3}\tilde{a})\mathbf{e}_x$. An expansion in $\mathbf{k} = \mathbf{q} \mp \mathbf{K}$, up to third order yields

$$h(+, \mathbf{k}) = \hbar v_F \left(k - \frac{\tilde{a}w_1}{4} k^{*2} - \frac{\tilde{a}^2 w_2^2}{8} |\mathbf{k}|^2 k \right) \quad (2)$$

$$h(-, \mathbf{k}) = -\hbar v_F \left(k^* + \frac{\tilde{a}w_1}{4} k^2 - \frac{\tilde{a}^2 w_2^2}{8} |\mathbf{k}|^2 k^* \right), \quad (3)$$

for the K ($\alpha = +$) and K' ($\alpha = -$) points, respectively, where we have used the complex notation $k = k_x + ik_y$ and $v_F = 3t\tilde{a}/2\hbar$. Furthermore, we have introduced the phenomenological parameters w_1 and w_2 , in order to account for corrections beyond the simplest tight-binding model [19], which yields $w_1 = w_2 = 1$. For the n.n.n. term, expanded to lowest non-trivial order around K and K' , one obtains

$$h'(\mathbf{k}) = -3t' + \frac{9t'\tilde{a}^2}{4}(k_x^2 + k_y^2) \quad (4)$$

and thus the total energy dispersion, taking into account

both higher-order band corrections and n.n.n. hopping,

$$\varepsilon_{\sigma=\pm}^{\alpha=\pm}(\mathbf{k}) = \hbar v_F \left\{ \sigma |\mathbf{k}| \left[1 - \alpha \frac{\tilde{a} w_1 |\mathbf{k}|}{4} \cos 3\phi_{\mathbf{k}} - \frac{\tilde{a}^2 |\mathbf{k}|^2}{32} (4w_2^2 - w_1^2 + w_1^2 \cos^2 3\phi_{\mathbf{k}}) \right] + \frac{3t'}{2t} \tilde{a} |\mathbf{k}|^2 \right\}, \quad (5)$$

where $\sigma = +$ denotes the conduction and $\sigma = -$ the valence band, and $\tan \phi_{\mathbf{k}} = k_y/k_x$. We have subtracted the unimportant constant $-3t'$, redefining the zero-energy position. The cosine terms in Eq. (5) indicate that the energy dispersion becomes anisotropic (trigonal warping) [19]. One clearly notices from Eq. (5) that n.n.n. hopping breaks the particle-hole symmetry but leaves the Fermi velocity unchanged.

In order to account for the magnetic field, we use the Peierls substitution, which consists of replacing the wave vector \mathbf{k} by a momentum operator in the continuum minimally coupled to the vector potential \mathbf{A} , $\mathbf{k} \rightarrow \mathbf{\Pi} = \mathbf{p} + e\mathbf{A}$ [20]. The operator $\mathbf{\Pi}$ may be expressed in terms of harmonic-oscillator ladder operators, with $[a, a^\dagger] = 1$, and the Peierls substitution thus reads

$$k \rightarrow i\sqrt{2}l_B^{-1}a^\dagger \quad \text{and} \quad k^* \rightarrow -i\sqrt{2}l_B^{-1}a. \quad (6)$$

Here, $l_B = \sqrt{\hbar/eB} = 26/\sqrt{B[T]}$ nm is the magnetic length, which is large in comparison with \tilde{a} , and the above corrections to the linear energy dispersion are governed, in the presence of a magnetic field, by the small parameter \tilde{a}/l_B . The substitution (6), together with Eqs. (2)-(4), allows one to calculate the energies of the relativistic LLs, which, in the absence of the trigonal-warping terms, read

$$\gamma^2 \left[n - \frac{4w_2^2 - w_1^2}{8} \left(\frac{\tilde{a}}{l_B} \right)^2 n^2 \right] = \left(\varepsilon_n - \gamma \frac{3t'\tilde{a}}{\sqrt{2}tl_B} n \right)^2. \quad (7)$$

Here, we have defined $\gamma \equiv \sqrt{2}\hbar v_F/l_B$ and neglected terms due to the order of the operators a and a^\dagger when using the substitution (6). This is justified in the large- n (semiclassical) limit. In order to account for trigonal-warping at leading order, we use perturbation theory, which is justified because $\tilde{a}/l_B \ll 1$. There is no contribution at first order since $\langle n|a^{(\dagger)3}|n \rangle = 0$ due to the orthogonality of the eigenstates $\langle n|n' \rangle = \delta_{n,n'}$. At second order, one obtains $-\gamma^2 w_1^2 (\tilde{a}/l_B)^2 [3n(n+1) + 2]/8$, which needs to be added to the l.h.s. in Eq. (7). The fact that trigonal warping is manifest only at order $(\tilde{a}/l_B)^2$ is due to the magnetic field, which averages to zero the $\cos 3\phi_{\mathbf{k}}$ term in Eq. (5) when summing over the angle $\phi_{\mathbf{k}}$.

One finally obtains, in the large- n limit, where these corrections become relevant, the energies of the relativistic

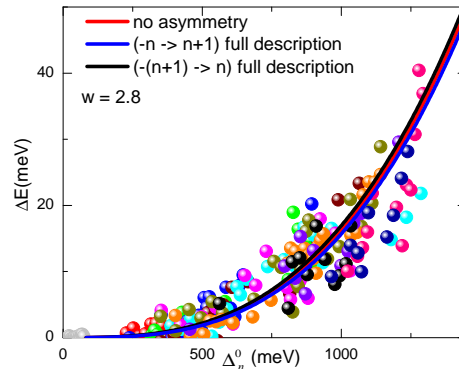


FIG. 2: (color online) The deviation from linearity ΔE (from the data in Fig. 1(b), with the same colors) for the different transitions as a function of the energy Δ_n^0 . The solid lines is the result of the theoretical calculation as described in the text.

tic LLs for both valleys, K and K' ,

$$\varepsilon_{\sigma,n} = \gamma \frac{3t'}{\sqrt{2}t} \frac{\tilde{a}}{l_B} n + \sigma \gamma \sqrt{n} \left\{ 1 - \frac{3w^2}{8} \left(\frac{\tilde{a}}{l_B} \right)^2 [n + \mathcal{O}(n^0)] \right\}, \quad (8)$$

where $\mathcal{O}(n^0)$ stands for corrections of order unity, and we have defined $w^2 \equiv (w_1^2 + 2w_2^2)/3$, which may be measured experimentally. The LL structure in the presence of n.n.n. hopping has been discussed before in Ref. [21]. We have checked the above result within the semiclassical Onsager quantization scheme, and a comparison with a numerical solution of the Harper equation on the honeycomb lattice shows excellent agreement even at small values of n [22].

In our experimental study, we compare the deviation $\Delta E^\pm = \Delta_n^0 - \Delta_n^\pm$ between the interband-transition energies $\Delta_n^0 = \gamma(\sqrt{n+1} + \sqrt{n})$ of the ideal case of Dirac electrons with linear dispersion and the measured transitions Δ_n^+ (for $-n \rightarrow (n+1)$) and Δ_n^- (for $-(n+1) \rightarrow n$), as a function of Δ_n^0 . In Fig. 2, we compare these deviations to the theoretical expectations

$$\Delta E^\pm = \mp \frac{9t'}{2} \left(\frac{\tilde{a}}{l_B} \right)^2 + \frac{3\tilde{a}^2 w^2}{64\hbar^2 v_F} (\Delta_n^0)^3, \quad (9)$$

obtained from Eq. (8) in the large- n limit and $\Delta_n^\pm = \pm(\varepsilon_{\pm,n+1} - \varepsilon_{\mp,n})$. Note that $\Delta_n^0 \propto \sqrt{Bn}$ when $n \gg 1$. The solid lines in Fig. 2 show the theoretical result (9) with a fitting parameter $w = 2.8$ (compared to $w = 1$ in the simplest tight binding model). This somewhat large value indicates that although the tight-binding model yields the correct functional form and order of magnitude of band corrections, it underestimates the strength of these corrections, in particular the effect of the trigonal warping. In order to account for this enhanced value in a theoretical model, one would need to include corrections due to the overlap of the atomic wave-functions on the

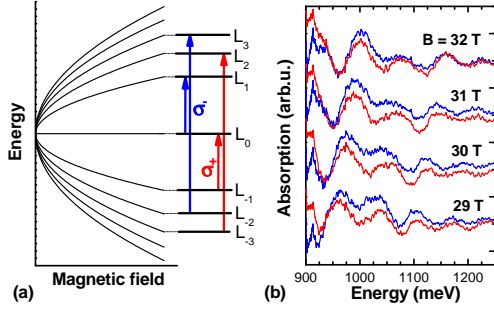


FIG. 3: (color online) (a) The polarization selection rules for optical transitions in graphene. (b) The differential transmission spectra for both circular polarization of the light.

different lattice sites, larger distance hopping, and possibly interaction effects. One may also speculate that, although the graphene layers are only weakly coupled, the remaining interlayer coupling might play a role [23]. Indeed, trigonal warping in bilayer graphene and graphite is dominated by *interlayer* hopping, which could be on the same order of magnitude as the abovementioned dispersion corrections [24, 25].

Eq. (8) shows that the LLs are not electron-hole symmetric due to n.n.n. hopping. The resulting asymmetry $\mathcal{A} \equiv |\Delta_n^- - \Delta_n^+|$ in optical LL transitions is $\mathcal{A} = 3\sqrt{2}\gamma t' \tilde{a} / t l_B \simeq 0.08 B [T] \text{ meV}$, which is independent of n . At fields as high as 30 T, one therefore expects an electron-hole asymmetry on the order of 2.5 meV, which roughly corresponds to the thickness of the theoretical curve in Fig. 2. The effect is thus beyond the resolution of our experimental data.

Additional confirmation of the small electron-hole asymmetry in the LL transitions can be seen using a polarization-resolved experiment. The polarization selection rules for optical transition in graphene are shown schematically in Fig. 3(a). In Fig. 3(b) we present transmission spectra measured for both polarizations at different magnetic field values. No significant differences between the positions of the absorption lines can be seen for the different polarization suggesting that there is no observable asymmetry between the electron and hole cones.

Symmetry breaking in a gated single sheet of graphene has been reported recently by Deacon *et al.* [12]. In their cyclotron resonance measurements, the asymmetry is attributed to n.n. wave-function overlap corrections characterized by the overlap integral s_0 [26]. In this case the LL transition asymmetry is $\mathcal{A}' = 3\sqrt{2}\gamma s_0 \tilde{a} / l_B \propto B$, which shows that s_0 plays a role similar to t'/t , even though the two types of asymmetry have different microscopic origins. Deacon *et al.* estimated the strength of the asymmetry to be $\mathcal{A}' \simeq 5 \text{ meV}$ at $B \simeq 9 \text{ T}$ from the $0 \rightarrow 1$ and $-1 \rightarrow 0$ transitions [12], which is in between 5 and 7 times larger than theoretical estimates, depending on whether one takes $s_0 = 0.129$ [26] or $t'/t \sim 0.1$

[18] with $t \approx 3 \text{ eV}$. For a field of 32 T, this would yield an asymmetry of the order of 18 meV, which should be visible, but is clearly not observed in the 32T spectra in Fig. 3(b).

In conclusion, we have probed the high-energy range ($\leq 1.25 \text{ eV}$) of the Dirac cone in multi-layer graphene and observed a significant deviation from the linear dispersion for massless Dirac fermions. A theoretical model which includes higher order band terms gives good agreement with experiment. No electron-hole asymmetry in interband-LL excitations is observed, in agreement with our theoretical description, where this asymmetry plays a minor role as compared to trigonal warping of the Fermi surface and higher order band corrections.

We thank P. Dietl, F. Piéchon and G. Montambaux for their numerical solution of the Harper equation on the honeycomb lattice. This work was partially supported by contract ANR-06-NANO-019.

-
- * Electronic address: Paulina.Plochocka@grenoble.cnrs.fr
- [1] K. S. Novoselov *et al.*, Nature **438**, 197 (2005).
 - [2] Y.-W. Tan, H. L. Stormer, and P. Kim, Nature **438**, 201 (2005).
 - [3] K. S. Novoselov *et al.*, Nature Phys **2**, 177 (2006).
 - [4] A. K. Geim and K. S. Novoselov, Nature Materials **6**, 183 (2007).
 - [5] M. I. Katsnelson, K. S. Novoselov, and A. K. Geim, Nature Physics **2**, 620 (2006).
 - [6] A. C. Ferrari *et al.*, Phys. Rev. Lett. **97**, 187401 (2006).
 - [7] D. Graf *et al.*, Nano Lett. **7**, 238 (2007).
 - [8] J. Yan, Y. Zhang, P. Kim, and A. Pinczuk, Phys. Rev. Lett. **98**, 166802 (2007).
 - [9] C. Faugeras *et al.*, arXiv:0709.2538 (2007).
 - [10] M. L. Sadowski, G. Martinez, M. Potemski, C. Berger, and W. A. de Heer, Phys. Rev. Lett. **97**, 266405 (2006).
 - [11] Z. Jiang *et al.*, Phys. Rev. Lett. **98**, 197403 (2007).
 - [12] R. S. Deacon, K. C. Chuang, R. J. Nicholas, K. S. Novoselov, and A. K. Geim, Phys. Rev. B **76**, 081406 (2007).
 - [13] M. L. Sadowski, G. Martinez, M. Potemski, C. Berger, and W. A. de Heer, Sol. St. Comm. **143**, 123 (2007).
 - [14] C. Berger *et al.*, J. Phys. Chem. **108**, 19912 (2004).
 - [15] C. Berger *et al.*, Science **312**, 1191 (2006).
 - [16] J. Hass *et al.*, arXiv:0706.2134v1 (2007).
 - [17] P. R. Wallace, Phys. Rev. **71**, 622 (1947).
 - [18] J. Charlier, J. Michenaud, X. Gonze, and J. Vigneron, Phys. Rev. B **44**, 13237 (1991).
 - [19] T. Ando, J. Phys. Soc. Jpn. **74**, 777 (2005).
 - [20] M. O. Goerbig, R. Moessner, and B. Doucot, Phys. Rev. B **74**, 161407(R) (2006), Although the continuum limit is, strictly speaking, no longer well defined due to the fact that the vector potential is unbound, a more precise treatment via the Harper equation shows that it yields the correct results.
 - [21] N. M. Peres, F. Guinea, and A. H. C. Neto, Phys. Rev. B **73**, 125411 (2006).
 - [22] P. Dietl, F. Piéchon, and G. Montambaux, arXiv:0707.0219. (2007).

- [23] A. H. C. Neto, Phys. Rev. B **73**, 245426 (2006).
- [24] J. W. McClure, Phys. Rev. **108**, 612 (1957).
- [25] G. Dresselhaus, Phys. Rev. B **10**, 3602 (1974).
- [26] R. Saito, G. Dresselhaus, and M. S. Dresselhaus, Physical

Properties of Carbon Nanotubes (Imperial College Press, London, 1998).